# Analytical Modeling for the Design of a Piezoelectric Rotating-Mode Motor

Marc Budinger, Jean-François Rouchon, and Bertrand Nogarede

***Abstract*—This paper deals with the analytical modeling of a rotating-mode motor. The modeling, based on an equivalent electric circuit, is established by using geometrical and electromechanical parameters for the different parts of the motor. It gives electromechanical characteristics and other useful values for motor design. Numerical simulations and measurements from a real transducer validate the analysis.**

***Index Terms*—Analytical modeling, contact modeling, equivalent circuit, global modeling, piezoelectric motor, rotating-mode.**

## NOTATIONS

| | |
|---|---|
| $\Psi$ | Rotational angle. |
| $\omega$ | Frequency. |
| $\rho$ | Density. |
| $\gamma$ | Poisson constant. |
| $\mu$ | Friction constant. |
| $\varepsilon^S$ | Dielectric constant for constant $S$. |
| $A$ | Section area. |
| $a$ | Half length of contact (Hertz theory). |
| $a_T$ | Timoshenko's coefficient. |
| $C$ | Elastic stiffness. |
| $C_0$ | Clamped capacity. |
| $C^D$ | Elastic stiffness for constant-$D$. |
| $D$ | Electric displacement component along axe $x$. |
| $E$ | Electric field component along axe $x$. |
| $e$ | Piezoelectric constant. |
| $E_\theta$ | Equivalent voltage for tangential movement. |
| $E_r$ | Equivalent voltage for radial movement. |
| $F_{\text{pres}}$ | Effort on stator. |
| $G$ | Coulomb modulus. |
| $H$ | Piezoelectric constant. |
| $I$ | Moment of inertia. |
| $I$ | Current. |
| $K$ | Wave number. |
| $k$ | Coupling factor. |
| $L$ | Length of rod. |
| $L_n$ | Linear load (Hertz theory). |
| $M$ | Bending moment. |
| $N$ | Force factor. |
| $P$ | Contact pressure. |
| $P_\theta$ | Power of the tangential movement. |
| $P_0$ | Maximum pressure of contact (Hertz theory). |
| $P_r$ | Power of the radial movement. |
| $R$ | Cylinder radius. |
| $R_{eq}$ | Radius of equivalent cylinder (Hertz theory). |
| $S$ | Strain. |
| $T$ | Shear force. |
| $U, u$ | Displacement. |
| $V$ | Supply voltage |
| $W_c$ | Width of contact. |

Manuscript received June 23, 2001; revised May 16, 2002 and April 20, 2003.

The authors are with Laboratoire d'Electrotechnique et d'Electronique Industrielle, 31071 Toulouse, Cedex 7, France (e-mail: nogarede@leei.enseeiht.fr).

Digital Object Identifier 10.1109/TMECH.2004.823846

## I. INTRODUCTION

PIEZOELECTRIC actuators have certain advantages over alternative technologies, such as providing a high torque–mass ratio, locking when the supply is switched off and being less intrusive in use [1], [2]. Piezoelectric actuators would therefore appear to be an attractive option for biomedical applications. In this context, interdisciplinary research supported by the French government [3] aims at the development of a demonstrator of a motorised artificial hand based on piezoelectric actuators. This paper considers a piezoelectric actuator, suitable for the motorization of a prosthetic hand; in the form of rotating mode motor, constrained by its proposed application to a diameter of about 30 mm. To help with the design of this structure, an analytical modeling of its vibrating stator and of the stator/rotor contact is developed. The representation of the free vibrating stator is first presented. The contact interaction between stator and rotor is then introduced in the model. Results obtained from the analysis are validated by numerical and experimental results.

## II. ROTATING-MODE MOTOR

The rotating-mode motor is a cylindrical ultrasonic motor which is used by Canon to control some camera lenses [4], [5]. It was presented for the first time by [6] in centimeter size and it has also been designed in millimeter size [7], [8]. The work reported in literature on cylindrical motors mainly concerns design and fabrication technologies. A few papers deal with modeling: [10] gives a matrix method for analyzing a flexural vibration system, while [14] gives a kinematic analysis of the driving mechanism. The rotating-mode structure uses two orthogonal modes of bending of a cylindrical beam composed of piezoelectric ceramics sandwiched between two counter masses where the whole is axially prestressed by a screw. The mobile part is pressed against the extremity of the cylinder by a spring.

The ceramics used to excite the stator are discs with opposing polarization on each half. They are orthogonally placed to excite each mode of bending in order to create a traveling wave onto the end of the transducer (Figs. 1 and 2). They are supplied by sources of high frequency sinusoidal voltage (several tens

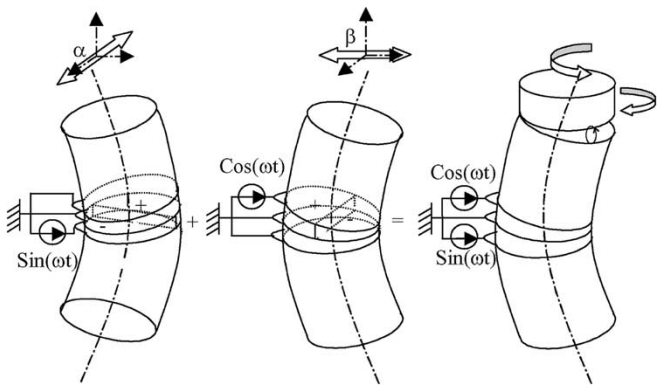


Fig. 1. Principle of the rotating-mode motor.

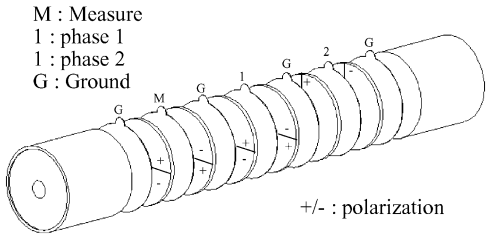


Fig. 2. Rotating-mode stator (exploded view).

of kilohertz) in quadrature. Fig. 2 shows a rotating-mode structure studied in the Laboratoire d'Electrotechnique et d'Electronique Industrielle (LEEI). The targeted torque is of the order to 0.3 N · m at 100 rev/min. Besides its simple structure and the good rotor/stator contact (permanent contact with distributed pressure), this motor also has the advantage of a stacked, prestressed structure which avoids expensive and delicate bonding operations and enables the use of the ceramics with a good coupling mode, and always under compression.

## III. Modeling of Rotating-Mode Motor Stator

The stator of the rotating-mode motor has the same assembly as that of a Langevin type transducer with its counter-mass, ceramics and pre-stressed screws. The difference comes from the nature of the excited modes; modes of flexion for the rotating-mode motor but longitudinal vibration modes for the Langevin type transducer.

### A. Equivalent Electric Circuit Modeling of Langevin Type Actuator

The Langevin type transducer is modeled in a classic way with Mason equivalent electric circuits [9]. Using the transducer geometry, they make it possible to get a relatively precise model of the electromechanical conversion based on a analogy between longitudinal vibratory speed and current (the counterpart of effort in one section is then voltage). According to this approach, a nonpiezoelectric rod in traction/compression can be modeled by the equivalent circuit of Fig. 3 where voltage $F$ and current $\dot{U}$, respectively, represent the effort and speed at the extremities of the rod. A transformer which expresses the electromechanical energy conversion is added to the circuit to take care of the piezoelectric ceramic effect.

### B. Modeling by Equivalent Circuits of the Stator

Following this approach, the model of the stator of a rotating-mode motor has been developed, which, in this case, lends itself to the calculation of the characteristic bending magnitudes and hence the angular vibratory speed and moment at a section.

*1) Equivalent Diagram in Flexion:* As a first stage, only ordinary elastic materials are modeled. To this end, an elementary cross section of a beam of section $A$ and of moment of inertia $I$ is isolated in Fig. 4. Displacement is orthogonal displacement ($u$) or rotation angle ($\Psi$). Effort is shearing ($T$) or moment ($M$). By applying the fundamental principle of dynamics to this elementary volume, we get

$$\rho A\frac{\partial^2 u}{\partial t^2} = -\frac{\partial T}{\partial x} \tag{1}$$

$$\text{and} \quad \rho I\frac{\partial^2 \psi}{\partial t^2} = \frac{\partial M}{\partial x} - T. \tag{2}$$

The elasticity equations of the materials give

$$\frac{\partial \psi}{\partial x} = \frac{M}{cI} \tag{3}$$

$$\text{and} \quad \psi - \frac{T}{a_T AG} = \frac{\partial u}{\partial x}. \tag{4}$$

The beams studied here are relatively short and the effects of the moment of inertia of the section, $\rho I dx(\partial^2\Psi/\partial t^2)$, and the shearing effect, $T/(a_T SG)$, will not be neglected [11]. For steady-state sinusoidal excitation and vibration the following complex notation can be adopted: $u = Ue^{j\omega t}$. The differential equation of propagation of the elastic wave is then

$$cI\frac{\partial^4 U}{\partial x^4} + \omega^2\rho I\left(1 + \frac{c}{a_T G}\right)\frac{\partial^2 U}{\partial x^2} + \left(\omega^4\frac{\rho^2 I}{a_T G} - \omega^2\rho S\right)U = 0. \tag{5}$$

This has a solution of the form

$$U(x) = A\sin(k_1 x) + B\cos(k_1 x) + Csh(k_2 x) + Dch(k_2 x). \tag{6}$$

To derive the characteristics of the stator, it will be treated as an isolated assembly (in this case, each end is free, with no shearing nor bending stresses). Starting from the general expression (6) of the orthogonal displacement $U$, the expression of the moments $M$, the angles $\psi$, and the shearing efforts $T$ are

$$M(x) = \alpha_M\left(A\sin(k_1 x) + B\cos(k_1 x)\right) + \beta_M\left(Csh(k_2 x) + Dch(k_2 x)\right) \tag{7}$$

$$\psi(x) = \alpha_\psi\left(A\cos(k_1 x) - B\sin(k_1 x)\right) + \beta_\psi\left(Cch(k_2 x) + Dsh(k_2 x)\right) \tag{8}$$

$$T(x) = \alpha_T\left(A\cos(k_1 x) - B\sin(k_1 x)\right) + \beta_T\left(Cch(k_2 x) + Dsh(k_2 x)\right). \tag{9}$$

By applying boundary conditions at the end sections $S_1$ and $S_2$ (shearing efforts $T_1$ and $T_2$ null) coefficients $A, B, C$, and $D$ can be determined as functions of angles $\psi_1$ and $\psi_2$. Once these

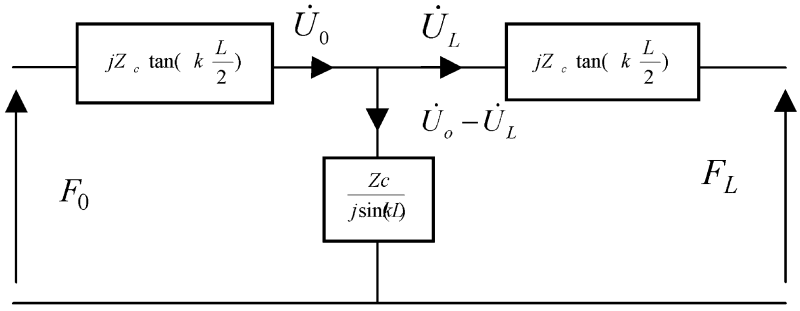


Fig. 3. Equivalent electric circuit of a nonpiezoelectric rod.

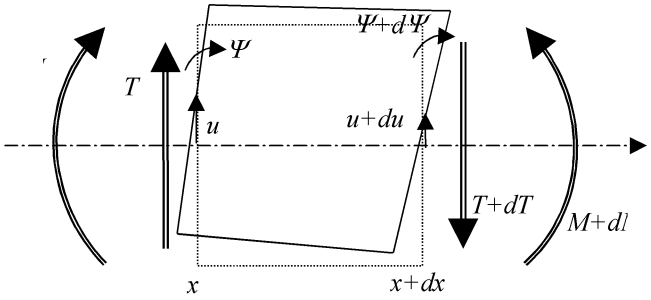


Fig. 4. Elementary cross section of a beam in flexion.

coefficients are determined, the expression of the moments can be written

$$M_1 = M\left(-\frac{L}{2}\right) = \tilde{\alpha}\dot{\psi}_1 + \tilde{\beta}\left(\dot{\psi}_1 - \dot{\psi}_2\right) \tag{10}$$

$$M_2 = M\left(+\frac{L}{2}\right) = -\tilde{\alpha}\dot{\psi}_2 + \tilde{\beta}\left(\dot{\psi}_1 - \dot{\psi}_2\right) \tag{11}$$

with

$$\tilde{\alpha} = \frac{\alpha_M\beta_T \tan\left(\frac{k_1L}{2}\right) - \beta_M\alpha_T \tanh\left(\frac{k_2L}{2}\right)}{j\omega\left(\alpha_\psi\beta_T - \beta_\psi\alpha_T\right)}$$

$$\tilde{\beta} = j\frac{\frac{\alpha_M\beta_T}{\sin(k_1L)} + \frac{\beta_M\alpha_T}{\sinh(k_2L)}}{\omega\left(\alpha_\psi\beta_T - \beta_\psi\alpha_T\right)}.$$

These equations can be put in the form of an electric equivalent circuit (Fig. 5) as for a Langevin type transducer [9].

It is also possible to represent this electric circuit by a matrix

$$\begin{pmatrix} M_2 \\ \dot{\psi}_2 \end{pmatrix} = \begin{pmatrix} 1+\frac{\tilde{\alpha}}{\tilde{\beta}} & -\tilde{\alpha}\left(2+\frac{\tilde{\alpha}}{\tilde{\beta}}\right) \\ \frac{-1}{\tilde{\beta}} & 1+\frac{\tilde{\alpha}}{\tilde{\beta}} \end{pmatrix} \begin{pmatrix} M_1 \\ \dot{\psi}_1 \end{pmatrix}. \tag{12}$$

*2) Equivalent Diagram of the Stator:* The stator is made up of ceramics and counter masses. Its total dynamic behavior can be also modeled by an equivalent diagram with $M$ and $\dot{\psi}$. To calculate this parameter, it will however be necessary to take into account the shearing forces present at the interfaces between the various parts of the stator. The equations of the preceding paragraph can be expressed by a fourth-order transfer matrix with

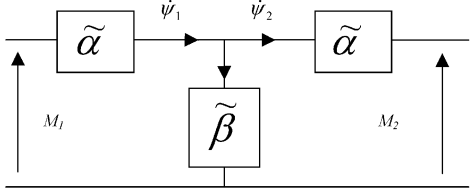


Fig. 5. Electric form equivalent circuit.

$M$, $\dot{\psi}$, $T$, and $\dot{U}$. The analytical expressions for its components are described in [10]. For a ceramic or a counter mass, we have

$$\begin{pmatrix} M_2 \\ \dot{\psi}_2 \\ T_2 \\ \dot{U}_2 \end{pmatrix} = (\mathrm{M}_{ij}) \begin{pmatrix} M_1 \\ \dot{\psi}_1 \\ T_1 \\ \dot{U}_1 \end{pmatrix}. \tag{13}$$

The assembly is done by multiplying the matrices of the various parts of the stator

$$(\mathrm{M}) = \prod_k (\mathrm{M}_k). \tag{14}$$

The resonant frequency can be found from this matrix. For this frequency, on the end surfaces, efforts are null ($T_1 = T_2 = 0$ and $M_1 = M_2 = 0$) and

$$\mathrm{M}_{12}\mathrm{M}_{34} = \mathrm{M}_{14}\mathrm{M}_{32}. \tag{15}$$

For the global matrix of the stator, the notation can be simplified. Indeed, on the end surfaces $T_1 = T_2 = 0$, we get

$$\dot{U}_1 = -\frac{1}{\mathrm{M}_{34}}\left(\mathrm{M}_{31}M_1 + \mathrm{M}_{32}\dot{\psi}_1\right). \tag{16}$$

The fourth-order matrix can be reduced to a second-order matrix with $M$ and $\dot{\psi}$

$$\begin{pmatrix} M_2 \\ \dot{\psi}_2 \end{pmatrix} = \begin{pmatrix} \mathrm{M}_{11} - \frac{\mathrm{M}_{14}\mathrm{M}_{34}}{\mathrm{M}_{34}} & \mathrm{M}_{12} - \frac{\mathrm{M}_{14}\mathrm{M}_{32}}{\mathrm{M}_{34}} \\ \mathrm{M}_{21} - \frac{\mathrm{M}_{24}\mathrm{M}_{31}}{\mathrm{M}_{34}} & \mathrm{M}_{22} - \frac{\mathrm{M}_{24}\mathrm{M}_{32}}{\mathrm{M}_{34}} \end{pmatrix} \begin{pmatrix} M_1 \\ \dot{\psi}_1 \end{pmatrix}. \tag{17}$$

$\tilde{\alpha}$ and $\tilde{\beta}$ can be calculated from this matrix and (12).

*3) Force Factor and Global Diagram:* When in movement with the structure assembled, deformations of the ceramics of the types in Fig. 6 have been observed (ANSYS) and it can then be assumed that the section stays flat and only pivots at an angle $\psi$.

As in longitudinal vibrations [9], the vibration is analyzed using a one-dimensional procedure along the $x$ axis and the electric field component $E$ cannot be assumed constant along

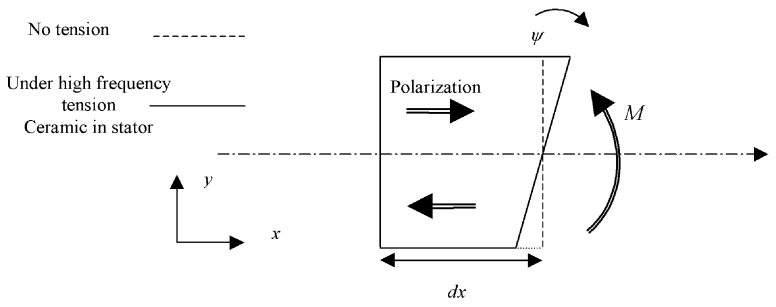


Fig. 6. Ceramic deformation.

the full length of the ceramic. On the other hand, the absence of free electric charge allows the writing of $\partial D/\partial x = 0$. Thus electric displacement $D$ here is a function of the ordinate $D(y)$. Effort $T$ is written

$$T(y) = c^D S(y) - hD(y) \tag{18}$$

$$\text{with } S(y) = \left(\frac{d\psi}{dx}\right) y. \tag{19}$$

As $D(y)$ is constant all along the ceramic, it is therefore equal to the average value along $x$. Starting from

$$D(y) = \varepsilon^S E(y) + eS(y). \tag{20}$$

By averaging on the length of the ceramic

$$D(y) = \langle D(y)\rangle = \varepsilon^S \langle E(y)\rangle + e\langle S(y)\rangle = \varepsilon^S \frac{V}{L} + e\frac{\psi_2 - \psi_1}{L} y. \tag{21}$$

Then, effort $T$ becomes

$$\begin{aligned} T(y) &= c^D \frac{d\psi}{dx} y - he\frac{\psi_2 - \psi_1}{L} y - h\varepsilon^S \frac{V}{L} \\ &= c^D \frac{d\psi}{dx} y - \frac{e}{\varepsilon^S}\frac{\psi_2 - \psi_1}{L} y - e\frac{V}{L}. \end{aligned} \tag{22}$$

By integrating $T(y)\cdot y$ on the surface of the ceramic, moment $M$ is deduced as

$$\begin{aligned} M &= \iint_{\text{section\_A}} T(y) y dA \\ &= c^D \frac{d\psi}{dx} \iint y^2 dA - \frac{e^2}{\varepsilon^S}\frac{\psi_2 - \psi_1}{L} \iint y^2 dA \\ &\quad - e\frac{V}{L} \iint |y| dA \end{aligned} \tag{23}$$

which can equally be written in the form

$$M + \frac{e^2}{\varepsilon^S}\frac{\psi_2 - \psi_1}{L} I + e\frac{V}{L} I_p = c^D I \frac{d\psi}{dx} \tag{24}$$

with

$$I = \iint y^2 dA \tag{25}$$

$$\text{and} \quad I_p = \iint |y|\, dA. \tag{26}$$

In (26), an expression of the form $M = cI(\partial\psi/\partial x)$ can be found again, and the supplementary terms are equivalent to a moment $\Gamma$. The force factor $N_{\text{cer}}$ for only the ceramic can then be deduced with

$$N_{\text{cer}} = \frac{e}{L} I_p. \tag{27}$$

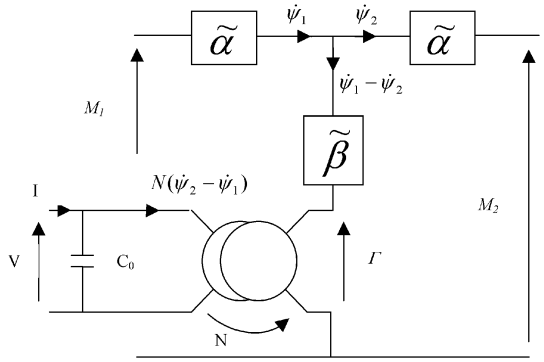


Fig. 7. Equivalent electric diagram of the stator.

Before introducing the transformer into the equivalent diagram of the stator, force factor should take account of the vibratory gain $G_v$ of the transducer between the piezoelectric materials and the end surfaces of the stator. This vibratory gain decreases efforts on end surfaces and is obtained with transfer matrix of a counter-mass. The global force factor is

$$N = \frac{N_{\text{cer}}}{G_v} = \frac{e}{G_v L} I_p. \tag{28}$$

The equivalent electric circuit for the stator is represented in Fig. 7, which includes the transformer to account for the electromechanical conversion at the level of the ceramic. The blocked capacity $C_0$ is expressed by

$$C_0 = \frac{\varepsilon^S A}{L}. \tag{29}$$

## IV. Modeling of Stator/Rotor Contact

To obtain the complete characteristics of the motor, it is necessary to add to the stator model, which describes the electromechanical power conversion, an analytical modeling of rotor/stator interaction. This stage has already been carried out for traveling-wave actuators [12], [13]. The vibration amplitude being supposed known, a study of the kinematics is now necessary.

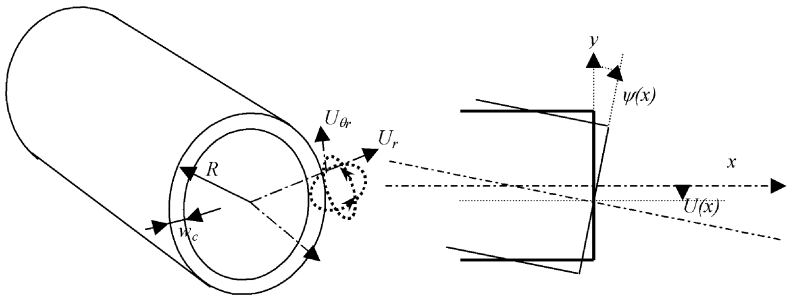


Fig. 8. Counter-mass deformation.

### A. Stator Kinematics

The expression of the rotating motor kinematics has been treated in [14]. It shows the existence of a traveling wave on the stator extremity. However, links with the equivalent circuit of the stator have to be established. Fig. 8 represents the deformations at the end of the cylinder for a bending movement. The phases of the motor are placed orthogonally and excite these modes of bending with a difference of phase of 90°. Thus, the deformations are as follows:

- For the first mode

$$\begin{cases} U_x^1 = -R\psi_0 \sin\theta \cdot e^{j\omega t} \\ U_y^1 = U_0 \cdot e^{j\omega t}. \end{cases} \tag{30}$$

- For the second mode

$$\begin{cases} U_x^2 = -R\psi_0 \cos\theta \cdot e^{j\omega t+(\pi/2)} \\ U_z^2 = U_0 \cdot e^{j\omega t+(\pi/2)}. \end{cases} \tag{31}$$

- For the sum

$$\begin{cases} U_x = -R\psi_0 e^{j\omega t+\theta+(\pi/2)} \\ U_z = U_0 \cdot e^{j\omega t} \\ U_z = U_0 \cdot e^{j\omega t+(\pi/2)}. \end{cases} \tag{32}$$

These deformations give (in cylindrical coordinates)

$$\begin{cases} U_r = U_0 \cos(\omega t+\theta) \\ U_\theta = U_0 \sin(\omega t+\theta) \\ U_x = R\psi_0 \cos(\omega t+\theta). \end{cases} \tag{33}$$

There is thus a traveling wave on the circumference of the stator. It is made up of two elliptic movements (Fig. 8):

- a first, tangential, and driving component, on $U_x$ and $U_\theta$;
- a second, radial, and undesirable component, on $U_x$ and $U_r$.

Contact with the rotor takes place for maximum $U_x$. The speeds of the elliptic movements at the time of the contact are

- $\begin{cases} \dot{U}_\theta = U_0\omega\cos(\omega+\theta) \approx U_0\omega \\ U_x = R\psi_0\cos(\omega t+\theta) \approx R\psi_0 \end{cases}$, for the useful movement
- $\begin{cases} U_r = U_0\omega c\sin(\omega+\theta) \approx 0 \\ U_x = R\psi_0\cos(\omega t+\theta) \approx R\psi_0 \end{cases}$, for the undesirable movement.

The undesirable movement has a zero or low speed at the time of the stator/rotor contact. The losses generated by this movement thus remain limited if the zone of contact is small.

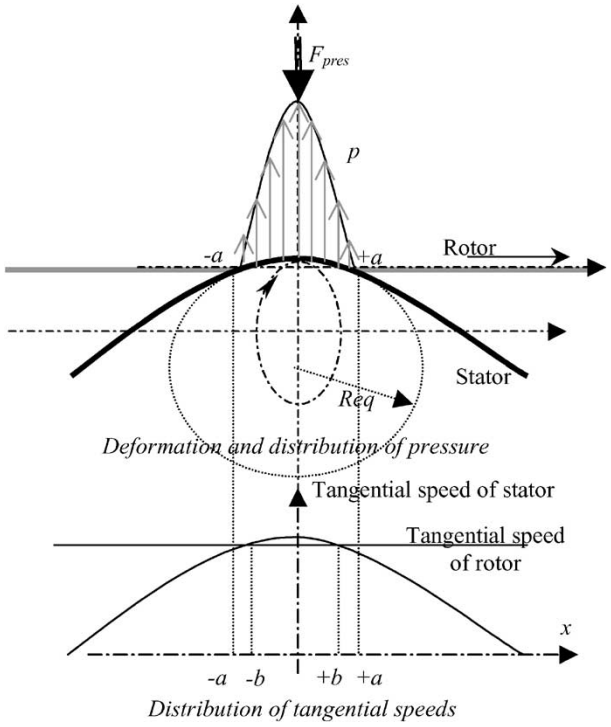


Fig. 9. Contact stator/rotor.

The relations between vibratory movements ($\psi$ and $U$) and elliptic movements have been established. The equivalent circuits are expressed according to angular vibratory speed $\dot{\psi}$. The circuit must also be able to account for the vibratory speed $\dot{U}$. This relation is given by (16)

$$\gamma = \frac{\dot{U}_1}{\dot{\psi}_1} = -\frac{\mathrm{M}_{32}}{\mathrm{M}_{34}}. \tag{34}$$

### B. Contact Between Stator and Rotor

*1) Zone of Contact:* The vibrating stator is assumed to be equivalent to a portion of a cylinder and the rotor to a plane surface. Thus the rotor/stator contact is equivalent to a cylinder/plane contact of length $2a$ and width $w_c$ (Fig. 9). Hertz's theory provides the length of contact and the distribution of pressure $p$.

Let $x$ be the position on the external perimeter of the stator (Fig. 8). The traveling-wave deformation $y$ has at $t = 0$

$$y = R\psi_0\cos(\theta) = R\psi_0\cos\left(\frac{x}{R}\right). \tag{35}$$

The radius of the equivalent cylinder $R_{eq}$ then takes the expression

$$R_{eq} = \left(\frac{\partial^2 y}{\partial x^2}\right)^{-1} = \frac{R}{\psi_0}. \tag{36}$$

The length of contact takes the value

$$a = 2\sqrt{\frac{L_n R_{eq}}{\pi E^*}} \tag{37}$$

with

$L_n = F_{\text{pres}}/c$ linear load;
$1/E^*$ $= (1-\gamma^2_{\text{stator}})/E_{\text{stator}} + (1-\gamma^2_{\text{rotor}})/E_{\text{rotor}}$ equivalent elasticity constant.

The distribution of pressure $p$ is given by

$$p = P_0\left(1-\left(\frac{x}{a}\right)^2\right)^{1/2} \text{ with } P_0 = \frac{2L_n}{\pi a}. \tag{38}$$

*2) Calculation of the Torque/Speed Curve for a Given Vibratory Speed:* The stator tangential speed $v$ is deduced from the tangential part $U_\theta$ of elliptic movement ($v$ is considered to be constant on the small width of contact $w_c$)

$$v = \dot{U}_\theta = U_0\omega\cos\left(\frac{x}{R}\right). \tag{39}$$

In Fig. 9, the coordinate $b$ corresponds to the point for which the local speed of the stator is equal to the tangential speed $\mathrm{V}_r$ of the rotor

$$V_r = \dot{U}_\theta = U_0\omega\cos\left(\frac{b}{R}\right) \text{ and } b = R\cdot\cos^{-1}\left(\frac{V_r}{U_0\omega}\right). \tag{40}$$

The efforts transmitted to the rotor depend on relative speed.

- For $v > V_r$ or $-b < x < b$, they are positive.
- For $v < V_r$ or $-\mathrm{a} < x < -b$ or $b < x < a$, they are negative.

By taking a law of friction of the type $dF = \mu\cdot p\cdot sg(v-V_r)dS$ (with friction coefficient $\mu$ constant), torque $C$ is calculated by

$$\begin{aligned} C &= 2\mu R\left(\int_0^b p(x)w_c dx - \int_b^a p(x)w_c dx\right) \\ &= 2\mu a w_c R P_0\left(\arcsin\left(\frac{b}{a}\right) + \frac{b}{a}\sqrt{1-\left(\frac{b}{a}\right)^2} - \frac{\pi}{4}\right). \end{aligned} \tag{41}$$

For low speeds ($b \geq a$), it takes the value

$$C_{\max} = \frac{\pi}{2}\mu a w_c R P_0 = \mu F_{\text{pres}} R. \tag{42}$$

Considering these expressions, the torque/speed characteristic is given by Fig. 10.

*3) Expression of the Mechano/Mechanic Conversion in the Equivalent Circuits:* For the points corresponding to the $b > a$ part of the characteristic (Fig. 10), the total power $P_\theta$ developed

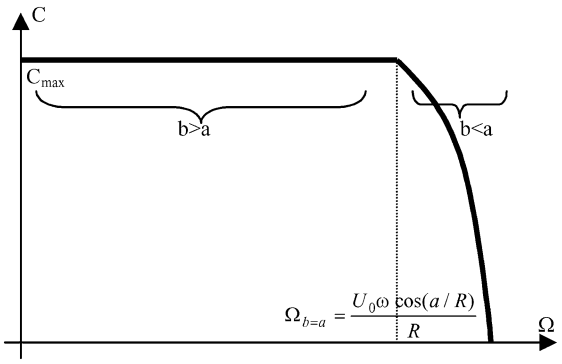


Fig. 10. Torque/speed characteristic.

in the contact for the tangential movement can be written in the following form:

$$\begin{aligned} P_\theta &= 2\mu\int_0^a p(x)\cdot w_c\cdot v(x)dx \\ &= 2\mu w_c U_0\omega P_0\int_0^a\sqrt{1-\left(\frac{x}{a}\right)^2}\cos\left(\frac{x}{R}\right)dx. \end{aligned} \tag{43}$$

If $\sqrt{1-(x/a)^2}$ is approximated by $\cos(\pi x/2a)$, $P_\theta$ becomes

$$P_\theta = \mu w_c U_0\omega P_0\cos\left(\frac{a}{R}\right)\frac{\pi a}{\left(\frac{\pi}{2}\right)^2-\left(\frac{a}{R}\right)^2}. \tag{44}$$

In equivalent circuits, the power $P_\theta$ could be calculated by

$$P_\theta = 2\frac{1}{2}\mathrm{Re}[M\dot{\psi}^*] = \mathrm{Re}[M\dot{\psi}^*]. \tag{45}$$

This expression can be rewritten according to (36)

$$\mathrm{Re}[M\dot{U}^*] = \mathrm{Re}[\gamma M\dot{\psi}^*] = \gamma\mathrm{Re}[M\dot{\psi}^*] = \gamma P. \tag{476}$$

Then

$$P = \frac{\mathrm{Re}[M\dot{U}^*]}{\gamma}. \tag{47}$$

As $\dot{U}_2$, $\dot{\psi}_2$, and $M_2$ are assumed to be co-phasal, the final expression of $M_2$ is

$$M_\theta = \frac{\gamma P}{U_0\omega} = \mu w_c\gamma P_0\cos\left(\frac{a}{R}\right)\frac{\pi a}{\left(\frac{\pi}{2}\right)^2-\left(\frac{a}{R}\right)^2}. \tag{48}$$

In the same way, for the radial movement, the power $P_r$ developed can be written. As for power $P_\theta$, this power corresponds to an analogous voltage $M_r$ given by

$$M_r = \mu w_c\gamma P_0 2a\frac{\frac{a}{R}-\left(\frac{\pi}{2}\right)\cdot\sin\left(\frac{a}{R}\right)}{\left(\frac{a}{R}\right)^2-\left(\frac{\pi}{2}\right)^2}. \tag{49}$$

The equivalent circuit (Fig. 11) of the motor can thus be supplemented by adding:

- a resistance $R$ to take account of the mechanical losses within the stator (this resistance can be replaced by the use of complex elastic constant [9]) ;
- a voltage $M_\theta$ to represent the power developed by tangential vibratory movement (48);

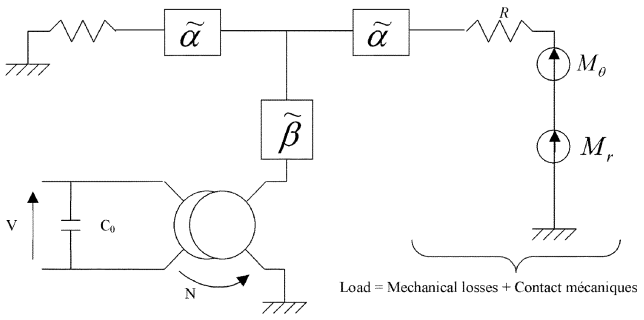


Fig. 11. Equivalent diagram of the motor.

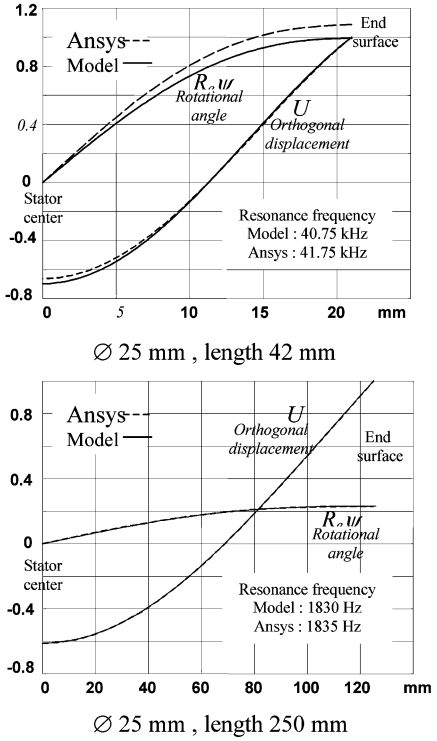


Fig. 12. Steel cylinder deformation at resonance frequency (half cylinder).

- a voltage $M_r$ to represent the power developed by tangential radial movement (49).

## V. Modeling Validation

First, we seek to check the dynamical part of the model in its ability to calculate the resonance frequency and the stator deformation. For this, we compare the results (Fig. 12) obtained by the model and a finite element method (FEM) software (ANSYS) on a steel cylinder for two configurations (long and short cylinder). In the case of the short cylinder (length/radius ratio lower than 3.5), which is the limiting value for beam modeling assumptions, the model gives a rather good precision: less than 3% of error on the frequency of resonance and less than 10% of error on rotational angle $\Psi$.

To validate the electromechanical modeling, we calculate the coupling coefficient $k$ for an elementary transducer (Two steel counter masses of 2-mm length and 25-mm diameter and two PC5H ceramics 1-mm thick): a variation of 7% is obtained between ANSYS and modeling results. One also notes for this geometry a difference of 10% on the level of the vibratory gain (8.5 model, 7.6 FEM).

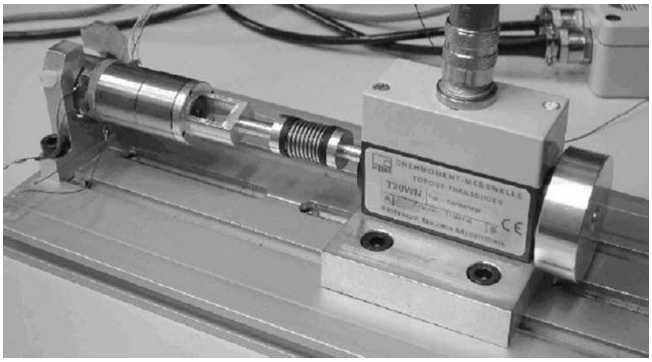

Fig. 13. Rotating-mode motor.

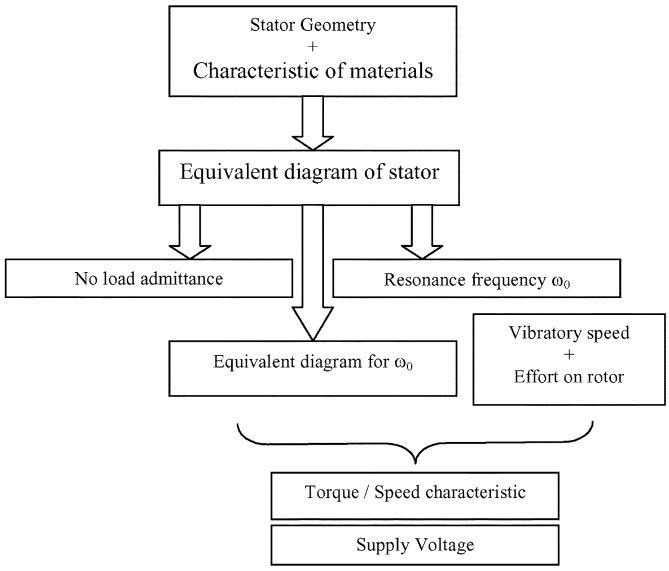


Fig. 14. Calculation of electromechanical characteristics.

For the global modeling, let us take the case of a rotating-mode motor (Fig. 13) made up of:

- two steel counter-masses;
- two phases of two ceramics (Morgan PC5H);
- one rotor placed against one of the counter-masses.

The equivalent circuit of the motor is as shown in Fig. 11. The electromechanical characteristics of this motor can be obtained by following the algorithm (Fig. 14) (programmed here with Matlab) which produces several useful results:

- no-load admittance of the stator, useful to obtain an equivalent electric representation of one motor phase (a great help in the design of the electronic amplifier);
- torque/speed curve;
- supply voltage and the maximum electric fields (risk of depolarization of ceramics);
- stress distribution, maximum stresses in ceramics (mechanical risk of rupture);
- motor efficiency.

An example of results is presented in Fig. 15 together with experimental points (*) on the torque/speed curve. The agreement between modeled and measured values is satisfying; differences

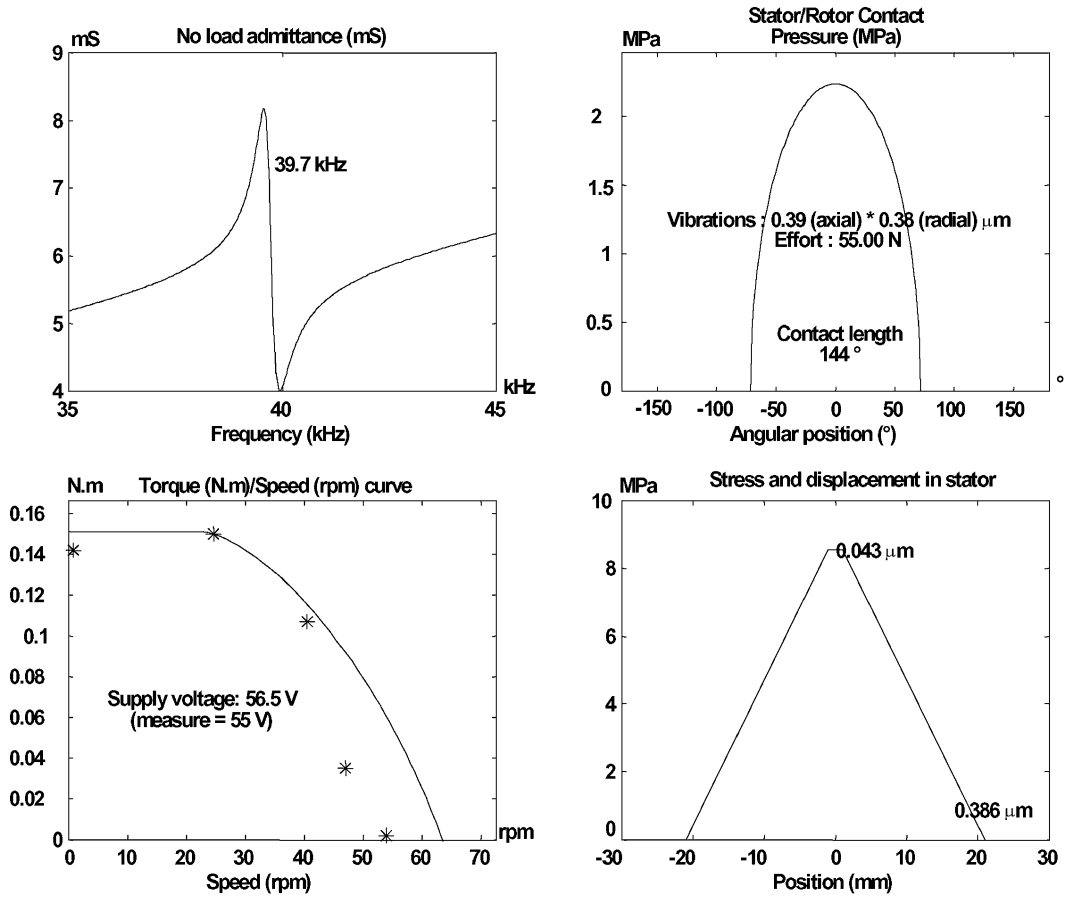


Fig. 15. Example of model results.

are due to the difference between calculated and real resonance frequency (10%) and to the nonlinearity of the friction coefficent around null slip speeds.

## VI. Conclusion

This paper has presented a global model for a cylindrical piezoelectric actuator as a rotating-mode motor taking into account both electromechanical conversion in the stator and mechano-mechanical conversion between stator and rotor. It has been shown that, for the free vibrating stator, a method based upon the Mason equivalent circuit is satisfactory. In order to take into account the assembly of the composite structure exciting in a flexural mode, a specific formulation using a transfer matrix including shear effects has been used. In the equivalent circuits, contact between rotor and stator can be represented by voltages which are functions of vibratory speed and these voltages can be calculated using the Hertz theory and associated with a constant friction coefficient between stator and rotor. The model has been implemented in a mathematical numerical environment (Matlab) and the global characteristic of the motor behavior, torque/speed curve, no-load admittance, supply voltage, stress and amplitude of vibrations, readily determined. When compared with FEM analysis, the results show satisfying accuracy (error of less than 10% for resonance frequency and for kinematics parameters). The experimental results obtained demonstrate the ability of the model to predict electromechanical global performance by using a rather simple analytical representation. An important possible aspect of the developed modeling is its power when used in an optimising design procedure [15] which requires a small amount of computation.

## Appendix
## Coefficients Used in (6)–(9)

$$k_1 = \sqrt{\frac{\sqrt{\Delta} + \rho I\left(1+\frac{c}{a_T G}\right)\omega^2}{2cI}}$$

$$k_2 = \sqrt{\frac{\sqrt{\Delta} - \rho I\left(1+\frac{c}{a_T G}\right)\omega^2}{2cI}}$$

$$\Delta = \left(\rho I\left(1+\frac{c}{a_T G}\right)\omega^2\right) + 4cI\rho S\omega^2\left(1-\frac{\rho I}{a_T SG}\omega^2\right)$$

$$\alpha_M = cI\left(\frac{\rho\omega^2}{a_T G} - k_1^2\right) \quad \beta_M = cI\left(\frac{\rho\omega^2}{a_T G} + k_2^2\right)$$

$$\alpha_\psi = \frac{k_1\left(\alpha_M + a_T SG\right)}{a_T SG - \rho I\omega^2} \quad \beta_\psi = \frac{k_2\left(\beta_M + a_T SG\right)}{a_T SG - \rho I\omega^2}$$

$$\alpha_T = a_T SG\left(\alpha_\psi - k_1\right) \quad \beta_T = a_T SG\left(\beta_\psi - k_2\right).$$

## References

[1] T. Sashida and T. Kenjo, *An Introduction to Ultrasonic Motors*. Oxford, U.K.: Clarendon, 1993.

[2] S. Ueha and Y. Tomikawa, *Ultrasonic Motors*. Oxford, U.K.: Oxford Science, 1993.
[3] B. Nogarede *et al.*, "Matériaux électroactifs et génie biomédical : Étude d'une prothèse de la main actionnée par une motorization piézoélectrique," in *Proc. MGE 2000*, Lille, France, Dec. 2000, pp. 27–31.
[4] *Vibration Driven Motor*, Canon, Santa Clara, CA, 1992.
[5] "Plaquette de présentation des optiques," Canon, Santa Clara, CA, 1992.
[6] M. Kurosawa *et al.*, "An ultrasonic motor using bending vibrations of a short cylinder," *IEEE Trans. Ultrason. Ferroelect. Freq. Contr.*, vol. 36, pp. 517–521, Sept. 1989.
[7] T. Morita *et al.*, "Design of a cylindrical ultrasonic micromotor to obtain mechanical output," *Jpn. J. Appl. Phys.*, vol. 35, pp. 3251–3254, 1996.
[8] ——, "Cylindrical micro ultrasonic motor utilizing bulk lead zirconate titanate (PZT)," *Jpn. J. Appl. Phys.*, vol. 38, pp. 3347–3350, 1999.
[9] T. Ikeda, *Fundamentals of Piezoelectricity*. Oxford, U.K.: Oxford Science, 1996.
[10] G. Zhou, "The performance and design of ultrasonic vibration system for flexural mode," in *Ultrasonics*. New York: Elsevier Science, 2000, vol. 38, pp. 979–984.
[11] S. Timoshenko, *Résistance des Matériaux*. Paris, France: Dunod, 1977.
[12] P. Minotti *et al.*, "Moteur piezo-électrique à onde progressive : I. Modélization de la conversion d'énergie mécanique à l'interface stator/rotor," *J. Phy. III*, vol. 6, no. 10, pp. 1315–1337, 1996.
[13] J. F. Rouchon and P. Kapsa, "The elastic contact area between a sinusoidal indentor and a layered solid : Application to calculation of ultrasonic motors performances," in *Proc. Int. Tribology Conf.*, Yokohama, Japan, Oct./Nov. 1995.
[14] P. Lu *et al.*, "A kinematic analysis of cylindrical ultrasonic micromotors," *Sens. Actuators A, Phys.*, vol. 87, pp. 194–197, 2001.
[15] F. Messine, B. Nogarede, and J.-L Lagouanelle, "Optimal design of electromechanical actuators : A new method based on global optimization," *IEEE Trans. Magn.*, vol. 34, pp. 299–308, Jan. 1998.

**Marc Budinger** was born in Mt. St. Martin, France, in 1975. He received the Agregation degree in applied physics from the ENS Cachan, Paris, France, in 1998. He received the DEA and the Ph.D degrees in electrical engineering from the Institut National Polytechnique de Toulouse, Toulouse, France, in 2000 and 2003, respectively.

He is currently with the Laboratoire d'Electrotechnique et d'Electronique Industrielle (LEEI) Toulouse, France. His current research activities include design and power supply of piezoelectric actuators.

**Jean-François Rouchon** was born in Lyon, France in 1966. He received the Ph.D. degree in mechanical engineering from Ecole Centrale de Lyon, Lyon, France, in 1996.

Since 1998, he has been with the Laboratoire d'Electrotechnique et d'Electronique Industrielle (LEEI) Toulouse, France, and Ecole Nationale Supérieure d'Electrotechnique, d'Electronique, d'Informatique, d'Hydraulique et des Télécommuncations (ENSEEIHT), Toulouse, France, where he is currently a Lecturer in the Electrical Engineering Department. His research interests include tribology of contact and design of electroactive structure.

**Bertrand Nogarede** was born in Montpellier, France, in 1964. He received the Dipl. Ing. degree in electrical engineering from Ecole Nationale Supérieure d'Electrotechnique, d'Electronique, d'Informatique, d'Hydraulique et des Télécommuncations (ENSEEIHT), Toulouse, France, and the Ph.D. degree from the Institut National Polytechnique de Toulouse (INPT), Toulouse, France, in 1987 and 1990, respectively.

He is currently a Professor in the Electrical Engineering Department of INPT/ENSEEIHT, where he teaches electrodynamics and electrical machines. He is also the Head of the Electroactive Machines and Mechanisms Research Group of INPT/ENSEEIHT and Laboratoire d'Electrotechnique et d'Electronique Industrielle (LEEI), Toulouse, France. The group consists of six permanent academics working in the fields of electromechanical energy conversion, with particular interest in novel techniques and design methodologies such as electroactive materials, composite magnetic materials, electroactive fluids, analytical field calculation, optimal design.